Helmholtz-Zentrum
Geesthacht
Zentrum für Material- und Küstenforschung

Final Draft
of the original manuscript:

Ofoegbu, S.U.; Yasakau, K.; Kallip, S.; Nogueira, H.I.S.; Ferreira, M.G.S.; Zheludkevich, M.L.:
Modification of carbon fibre reinforced polymer (CFRP) surface with sodium dodecyl sulphate for mitigation of cathodic activity.
In: Applied Surface Science. Vol. 478 (2019) 924 – 936.
First published online by Elsevier: 04.02.2019

https://dx.doi.org/10.1016/j.apsusc.2019.02.024

Modification of Carbon Fibre Reinforced Polymer (CFRP) Surface with Sodium Dodecyl Sulphate for Mitigation of Cathodic Activity.

Stanley Udochukwu Ofoegbu[1a], Kiryl Yasakau[a], Silvar Kallip[a], Helena I.S. Nogueira[b], M.G.S. Ferreira[a], M.L. Zheludkevich[c,d]

[a]*Department of Materials and Ceramic Engineering, CICECO-Aveiro Institute of Materials, University of Aveiro,* Campus Universitário de Santiago, *3810-193 Aveiro, Portugal.*

[b]*Department of Chemistry, CICECO-Aveiro Institute of Materials, University of Aveiro,* Campus Universitário de Santiago, *3810-193 Aveiro, Portugal.*

[c]MagIC-Magnesium Innovation Center, Institute of Materials Research, Helmholtz-Zentrum Geesthacht, Max-Planck-Strasse1 ,21502 Geesthacht, Germany.

[d]Institute for Materials Science, Faculty of Engineering, Kiel University, Kiel, 24103, Germany.

Abstract

Suppression of electrochemical activity (cathodic activity) on CFRP surface at cathodic potentials consistent with galvanic coupling of CFRP with active metals like aluminium and zinc have been demonstrated by electrochemical treatment of CFRP surface in the presence of sodium dodecyl sulphate (SDS). Modification to the CFRP surface by SDS adsorption was established using electrochemical impedance spectroscopy, cyclic voltammetry, and confocal Raman spectroscopy and atomic force microscopy. Electrochemical test results indicate interaction of SDS with CFRP with persistent effects, manifesting in a sustained suppression of electrochemical activity even after washing the treated CFRP surface. Mitigation of CFRP degradation under cathodic polarization in the presence of SDS and/or after prior exposure to SDS was established from scanning electron microscopy. Based on results obtained herein, plausible mechanisms/configurations involved in SDS interaction(s) with carbon fibre surfaces of the CFRP composite (that most probably account for reduced cathodic activity) were postulated.

Keywords: CFRP, sodium dodecyl sulphate, surface modification, galvanic corrosion, cathodic reactivity, periodicity.

[1] Corresponding Author Email:ofoegbu.stanley@ua.pt (Stanley Ofoegbu) Tel: +351 915 248 642

1. Introduction

The electrochemical activity of carbon and carbon surfaces is well known and documented [1-11], and have been exploited in a variety of applications such as, addition of carbon additives to enhance electronic conductivity in composite cathodes for Li-ion batteries [12-15], as catalyst and support for electrochemical energy conversion [16-19], oxygen reduction reaction [20-22], and sonoelectrocatalysis [23-24].

Graphitic materials are reported to possess at least two distinct types of surface sites; the basal plane and edge plane sites [25-28]. Knowledge about the reactivity of basal and edge sites on carbon surfaces have been evolving, but literature reports have been contradictory with respect to the electrochemical activity of basal sites on carbon surfaces. Whereas earlier reports had largely suggested nil or very low activity of carbon basal sites [25,26,27,29,30-33] more recent reports employing "microscopic and nanoscopic techniques" have shown that the carbon basal sites are more electrochemically active than previously thought [34-45]. From our analysis of arguments from both sides, the consensus opinion appears to be that carbon basal sites are much more electrochemically active than previously thought, but significantly less active than the edge sites. For carbon fibres, it has been demonstrated that due to a high degree of preferred orientation introduced during different stages of the manufacturing process, the graphite basal planes can be predominantly oriented parallel to the fibre axis with edge sites predominating the fibre ends [25]. Such preferential abundance of the more electro-active edge sites at the carbon fibre ends is a plausible source of its enhanced electrochemical activity. Marked differences have been reported [46] in the values of the double layer capacitances of these two types of sites with higher values generally measured for edge sites ; 3 uF cm^{-2} for basal sites and 50-70 uF cm^{-2} for edge sites. This difference has been exploited as a diagnostic tool to monitor changes on carbon surfaces with respect to the relative concentration of these two sites, with increase in the values of measured double layer capacitance indicative of increase in the concentration of edge sites [25]. The electrochemical activities on carbon surfaces involve electron transfer processes. The kinetics of these electron transfer processes on carbon materials can be ascribed to synergetic effects of its conductivity and surface chemistry, which can be characterized by the surface charge, surface C/O ratio, presence of quinone-like groups, and surface purity [47].

The stringent design requirements in the transport and other industries aimed at energy efficiency and environmental sustainability, promotes weight optimized design concepts in

which many materials are employed in individual products **[48-54].** In the aerospace and transport industries for instance, in addition to the use of ensembles of metals and alloys, incorporation of carbon fibre reinforced polymers (CFRP) in the design of products together with metals for increased structural efficiency have been on the increase with carbon fibre reinforced polymers envisaged to be capable of constituting more than 50% of the structural mass of aircrafts **[55]**. This expectation has been realized with Boeing´s roll-out of the 787 with 50% composite content by weight, up from 12% composite content by weight in the earlier 777, and Airbus´ use of 53% composite content in the A350XWB up from 10% in the A340 **[52,54,56-62]**. This beneficial trend is however prone to galvanic corrosion of metals in electrical contact with each other, or with CFRP which is known to support cathodic reactions on galvanic coupling to metals **[63-70]**, and electrochemical degradation of the composite **[71]**. In these structures, galvanic coupling of CFRP with metallic alloys is a possibility at structure edges, rivets, and joints on failure of sealing materials due to either age or service conditions, with implications on product efficiency, service life and safety. Galvanic coupling of CFRP to metallic alloys in the presence of electrolyte have been severally reported **[72-75]** to lead to accelerated anodic dissolution of the metal/alloy due to the well known CFRP´s ability to support cathodic reactions as a result of the presence of the electro-active carbon fibres **[65,74,76-77]**. In quiescent 50 mM NaCl solution limiting oxygen diffusion current densities in the range of ≈ 40 μA cm^{-2} have been reported for CFRP **[78]** which is estimated to be capable of supporting anodic dissolution rates of about 0.599, 0.436, and 0.132 mm yr^{-1} for zinc, aluminium, and iron respectively (of equal surface area) on galvanic coupling to CFRP **[78].** Consequently there arises a need for development of processes/procedures that can mitigate this ability of CFRP to actively support cathodic reactions at the cathodic polarizations it is subjected to, on galvanic coupling to metallic materials in composite structures.

In the light of the distinction between the electrochemical activity of two main surface sites on carbon surfaces **[25]**, it is obvious that the solutions to mitigating the un-wanted electrochemical activity of carbon in carbon-fibre reinforced polymers coupled to metals in technologically vital applications in the aeronautical and transport industries can be either, the surface modification of the carbon to generate more of the electrochemically inactive basal plane sites, and/or the inactivation of the electrochemically active edge sites. The work reported herein is an effort in this regard, employing the latter approach in which a surfactant; sodium dodecyl sulphate (SDS) was employed, and observed to interact with CFRP surface resulting in a

sustained reduction in electrochemical activity of CFRP surface at cathodic polarizations in chloride media, even after rinsing the treated CFRP surface in distilled water.

In the present study, electrochemical methods complemented by surface analysis techniques (AFM and Raman spectroscopy) have been employed to study SDS interaction with a carbon containing composite surface with and without impressed cathodic polarization and the effect of this interaction on the electrochemical response of the CFRP surface.

2. Experimental

Solid pultruded cylindrical carbon fibre reinforced composite of diameter 8 mm made of carbon fibre Tenax HT 24 K with 65% fibre content, and epoxy vinyl matrix material produced by Modulor Material Total GmbH was used for this study. For electrochemical tests, a working electrode was prepared by cutting cylindrical pieces of height 10 - 15 mm from the as-received cylindrical material, attached to insulating conducting wire at one end, and mounted in a polymeric resin (Epokwick) so that the other flat end is free of resin. After the resin is cured, samples were removed and polished with progressively finer silicon carbide abrasive papers from grit size 220 to 2500, and rinsed in deionized water. At the beginning of a new sequence of tests the CFRP electrode surface was refreshed by progressively polishing with silicon carbide papers of grit size 400, 600, 800, 1200, and 2500 in that order.

Test electrolytes were prepared from analytical grade reagents (NaCl ≥ 99.8% and sodium dodecyl sulphate ≥ 99%) both from Sigma - Aldrich without further purification using Type 1 deionized water from a Millipore system (resisitivity > 18 MΩ-cm).

Electrochemical tests (electrochemical impedance spectroscopy, cathodic polarization, potentiodynamic polarization, and cyclic voltammetry) were done using an Autolab PGSTAT 302N potentiostat using a 3-electrode setup. Electrochemical impedance spectra was acquired from 100,000 to 0.01 Hz at 60 points distributed logarithmically. Cathodic polarization was effected at -1000 mV_{SCE}. Potentiodynamic polarization was effected 10 mV from OCP values after 1 hour immersion in test electrolyte with a potential step of 2.44 mV and a scan rate of 1 mV/s. Cyclic voltammetry was done with same potential step between -1000 mV and +100 mV (SCE) but at a faster scan rate of 50 mV/s after 1 hour of desired surface modification and another hour immersion in quiescent 50 mM NaCl solution post surface modification.

Surface image acquisition and analysis was done using a Hitachi SU-70 high resolution scanning electron microscope with a micro-analysis system for energy dispersion spectrometry X-ray / EDS, (Bruker model QUANTAX 400 and XFlash 4010 light-duty detector). Confocal Raman

spectroscopy was done using the 532 nm laser on a WITec alpa 300+ confocal Raman spectrometer system.

AFM studies were carried out in-situ on highly ordered pyrolytic graphite (HOPG) samples exposed to 50 mM NaCl solutions containing different concentrations of SDS (0 -20 mM SDS) with and without cathodic polarization. Prior attempts at AFM studies on the composite CFRP surface were unsatisfactory due to difficulties in obtaining composite surface of sufficient atomic flatness. AFM measurements were carried out using a commercial Veeco MultiMode AFM with a NanoScope IIIa controller and extended electronic module (software version v5.12r5) with a contact-mode liquid cell. The AFM piezo scanner model AS-12V was calibrated using reference silicon gratings purchased from Micromash with a 3 µm lateral pitch and a step height of 90 nm. Probes were made of oxide-sharpened silicon nitride (NP-S20 Veeco) with a reflective gold coating on the back side and a nominal spring constant of 0.06 N/m. The tips were irradiated by UV light (254 nm) for 60 minutes prior to the experiment. The fluid cell was filled with about 0.5 mL of a solution and left for about 60 minutes to reach thermal equilibrium before the measurement.

Imaging of micellar aggregates was performed at low force set points in the pre-contact repulsive force regime **[79,80]**. Force set points have been adjusted to generate the best contrast in the repulsive force regime. The following measurement parameters were employed: line frequencies of 5 Hz and low integral and proportional gains (typically about 0.5-1). Image optimization followed the procedure described in Ref. **[79]**. All presented AFM images represent deflection signal without any treatments apart from those used during the scanning. All dimensional measurements of surface features are an average of independent measurements on AFM maps. In estimation of periodicity in the AFM images in this work the Autocorrelation Function which employs the root mean square deviation of the heights σ and T - the autocorrelation length was employed. This treatment filter averages all the map features and we adjudge it to be better than the measurements of single profiles on AFM maps.

3. Results and Discussions

3.1. Results from electrochemical tests

Figure 1 presents the results of potentiodynamic polarization tests in quiescent 50 mM NaCl solution without and with sodium dodecyl sulphate(SDS) in six concentrations varying from 0.1 mM to 20 mM. The result indicates a concentration related marginal reduction in cathodic

current densities in virtually the entire studied potential range (from OCP to -2000 mV_{SCE}), in the presence of SDS, which is most significant in the non-diffusion limited region from OCP to about -200 mV. On the basis of these observations it is postulated that most probably due to the well known surfactant properties of SDS, it interacts with the CFRP surface in a manner that retards oxygen transport to the surface (lower limiting diffusion current density) and electron transport across the interface that results in lower current densities above -1600 mV_{SCE} cathodic potentials for the secondary cathodic reaction of water reduction with hydrogen evolution. Additionally, adsorption of SDS to the CFRP surface can suppress this cathodic reaction by inhibiting the atomic hydrogen re-combination step.

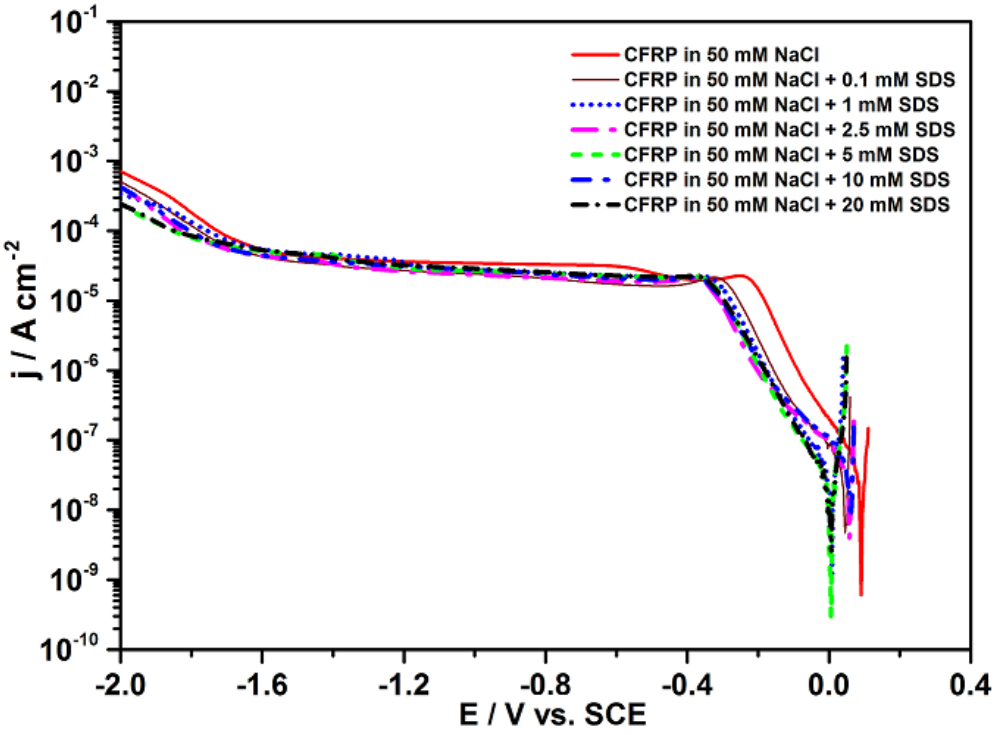

Fig. 1. Cathodic potentiodynamic polarization scans (scan rate 1 mV/s) on CFRP in 50 mM NaCl with different concentrations of sodium dodecyl sulphate (SDS).

To confirm the suppression of cathodic reactions by SDS interaction with CFRP surface, with and without prior cathodic polarization in the absence and presence of SDS, cyclic voltammetric tests were performed, and the response to cathodic activity on CFRP surface monitored through the well known cathodic reaction around -250 mV_{SCE} attributed to the 2-electron reduction of oxygen with formation of hydroxyl ions and hydrogen peroxide **[81]**.

From the comparative voltammograms of the first (**Fig.2a**) and second scans (**Fig.2b**), similar trends of significant reduction of this cathodic peak is confirmed (even on successive scans, **Fig.2a and 2b**) after exposure to SDS with and without the simultaneous application of a

cathodic polarization, compared to values in the absence of SDS after prior cathodic polarization. The smaller peaks observed in the absence of SDS (lemon green line) and prior to cathodic polarization (black line) indicates that prior exposure of CFRP surface to a cathodic polarization favours enhanced cathodic activity. This enhancement is attributed to the possible increase in electro-active surface area due to the degradative effect of the applied cathodic polarization (see SEM images ; **Fig. 6**).

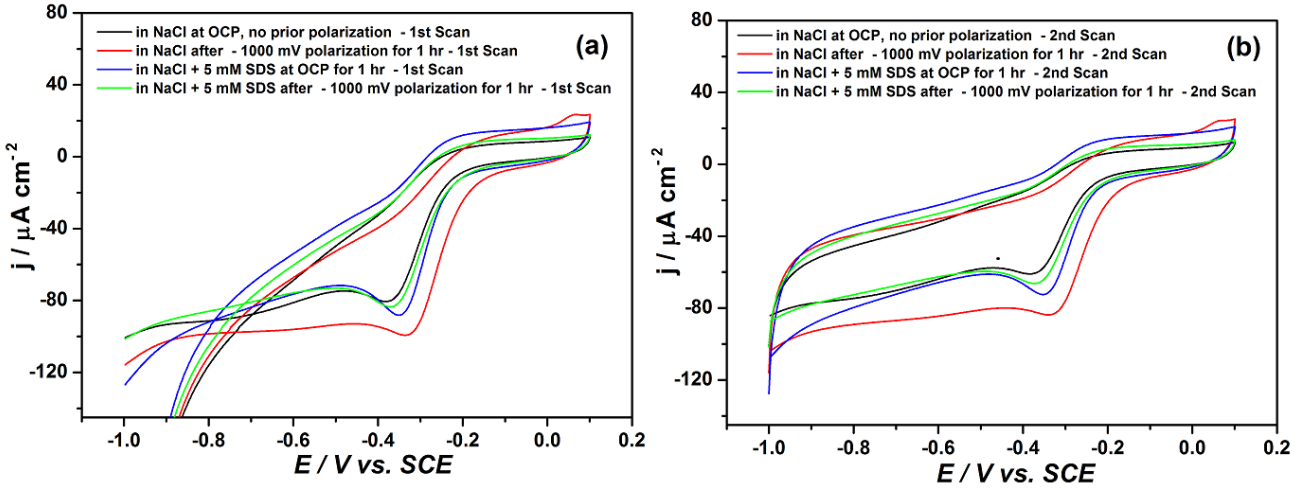

Fig.2. Cyclic voltammograms of CFRP in 50 mM NaCl without and after prior exposure to cathodic polarization in the presence and absence of SDS (scan rate 50 mV/s), (a) 1st scans and (b) 2nd scans.

To study the mechanism of the interaction of SDS with CFRP surface, electrochemical impedance spectroscopy was employed and spectra acquired from CFRP immersed in quiescent 50 mM NaCl with and without 5 mM SDS after different immersion times varying from 5 minutes to 24 hours with and without polarization (at OCP) presented as Bode and Nyquist plots (**Fig. 3**).

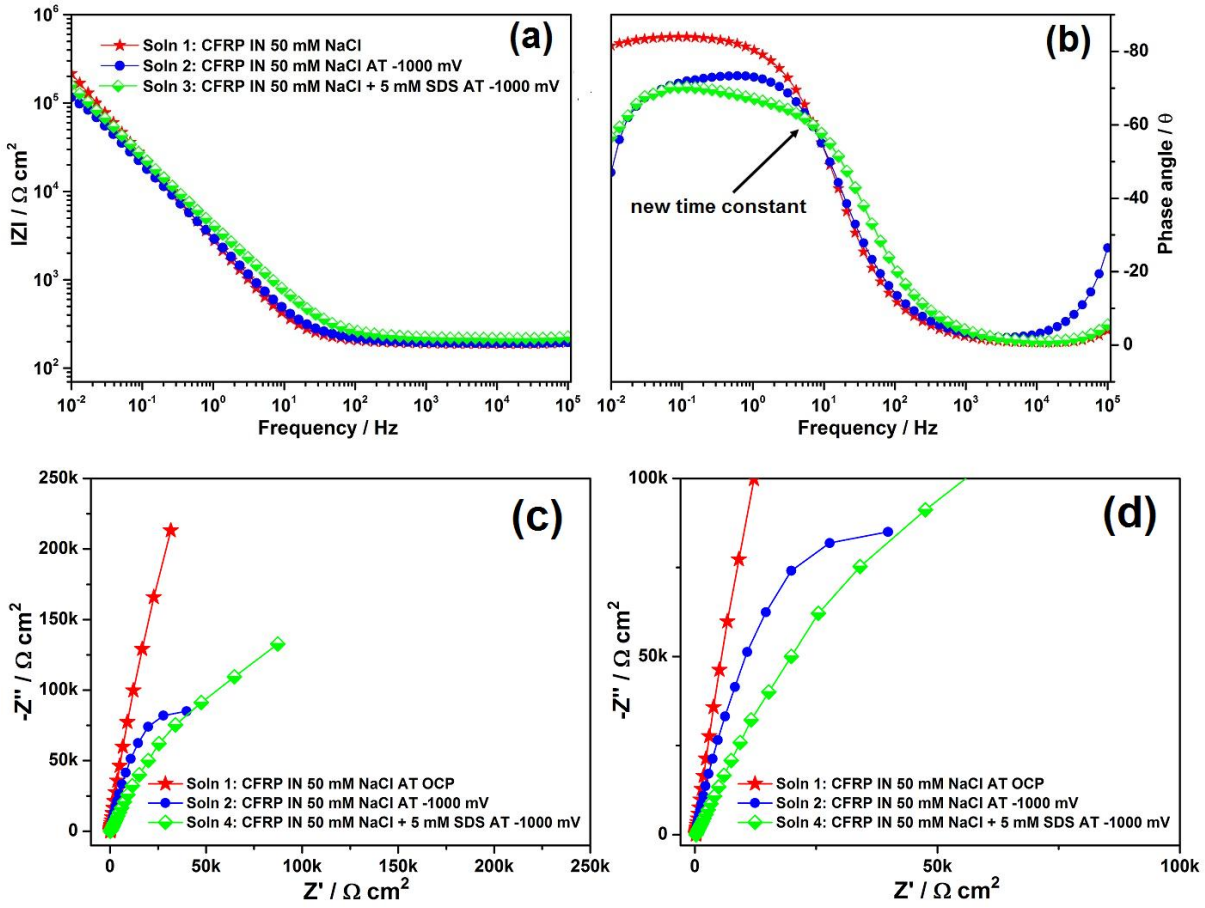

Fig. 3. Bode and Nyquist plots for CFRP in 50 mM NaCl without and with applied cathodic polarization of -1000 mV_{SCE} in the presence of 5 mM SDS.

The EIS spectra of CFRP in 50 mM NaCl + 5 mM SDS (**Fig. 3**) manifest two time constants. The mid-frequency time constant is attributed to SDS adsorption, and the low frequency time constant to charging of the double layer. Though the presence of this second time constant attributed to SDS adsorption on CFRP surface as it is not easily discernable from the Nyquist plots, (**Fig. 3c** and **3d**), its emergence is marked by increased asymmetry observable in mid to low frequency section of the angle phase vs frequency plot in the presence of both cathodic polarization and SDS (**Fig. 3b**, lemon green symbols), and the fact that the data fitted poorly to the one-time constant equivalent circuit (**Fig. 4d,** circuit 1**).** However, the inference of the existence of an emergent 2nd time constant is based on asymmetry observable in mid to low frequency section of the angle phase vs frequency plot and the fact that the data fitted poorly to the one-time constant equivalent circuit. Such trends can be observed in instances were an emerging time constant is small relative to the predominating time constant, and can be discriminated from each other by the application of impressed polarization which the potential sensitive time constant to be enhanced or suppressd relative to the other as for

instance in studies involving semi-conducting oxides on metal electrodes. This treatment was not possible in this instance because SDS adsorption on CFRP surface was not sensitive enough to changes in potential to permit such treatment.

The tests in the presence of SDS was done in triplicate. From **Fig. 3** it can be observed that the low frequency impedance in the presence of SDS and cathodic polarization of -1000 mV_{SCE} is consistently slightly higher than that in the presence of cathodic polarization but without SDS, but smaller than that in the absence of both (red symbol for measurement at OCP). It is concluded that under the applied cathodic polarization, the presence of SDS impedes composite electrochemical activity.

To confirm if these observed effects can be sustained outside the SDS (inhibitor) containing solutions, 3 sets of sequential immersion and EIS tests were carried out after immersion and testing in SDS containing solutions in 50 mM NaCl. In the first sequential test the EIS spectra of CFRP is acquired in 50 mM NaCl containing 5mM SDS after 1 hour immersion without any cathodic polarization (solution 3), and then in 50 mM NaCl only after another hour immersion without any cathodic polarization (solution 4). The aim was to establish whether the inhibitive effects observed after immersion in SDS containing solutions at OCP is sustained in aggressive media in the absence of inhibitors. In the second sequential test, the EIS spectra of CFRP is acquired in 50 mM NaCl containing 5mM SDS after 1 hour immersion under a cathodic polarization of -1000 mV_{SCE} (solution 5), and again after 1 hour immersion in the same solution but without cathodic polarization (solution 6). In the third sequential test, the EIS spectra of CFRP is acquired in 50 mM NaCl containing 5mM SDS after 1 hour immersion under a cathodic polarization of -1000 mV_{SCE} (solution 7), and then in 50 mM NaCl after another hour immersion with a sustained cathodic polarization of -1000 mV_{SCE} (solution 8). The aim of this sequence of tests was to confirm if inhibitive effects in SDS containing solutions under cathodic polarization are sustained on exposure under cathodic polarization in uninhibited solutions. Prior to transfer to a new test solution the sample was washed by dipping severally in distilled water and under a jet of distilled water. The results from these sequential EIS tests are presented in **Fig. 4**. For clarity, the Nyquist and Bode plots from solutions 1-5 are presented in **Fig.4a** and **4b** **r**espectively, while the others are included in the plots in the accompanying supplementary material (**S1** and **S2**).

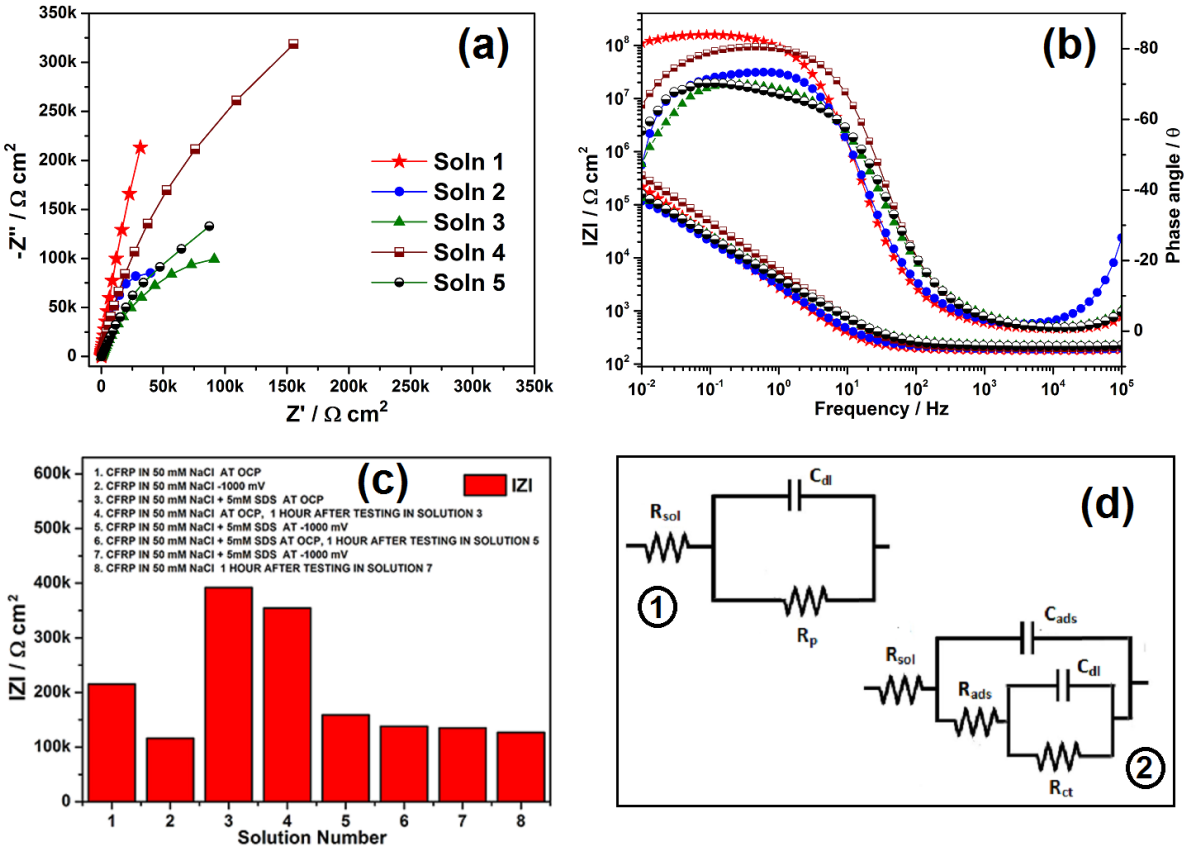

Fig. 4. Measured EIS data from sequential tests on CFRP, (a) Nyquist plots, (b) Bode plots, (c) low frequency impedance at 10^{-2} Hz, and (d) equivalent circuits used to fit impedance spectra.

Nyquist and Bode plots (**Fig. 4a** and **4b**, and supplementary materials **S1** and **S2**) indicate a reduction in capacitive response of CFRP on polarization with or without SDS (solutions 2, 5, and 7) compared to trends at OCP (Solution 1 and 4). From **Fig. 4c**, it is observed that a marked improvement is obtained in the low frequency impedance in the presence of SDS and without any polarization (solution 3) and sustained after washing in distilled water and testing in 50 mM NaCl without an applied cathodic polarization (solution 4) compared to values obtained in 50 mM NaCl (solution 1) without prior immersion in SDS containing solution. This results indicate that the inhibitive effects obtained by immersion in SDS containing solution at OCP is sustained on removal from the inhibitor solution and on exposure to aggressive media. Comparing low frequency impedance values (IZI at 10^{-2} Hz) measured in solutions 5 and 6 with that measured in solution 2 in **Fig. 5a**, it is observed that addition of 5 mM SDS to 50 mM NaCl causes an increase in the measured low frequency impedance even under a cathodic polarization of -1000 mV_{SCE} (solution 5) compared to the value obtained in uninhibited solution under cathodic polarization (solution 2). On re-testing the sample in same inhibited solution after a further 1 hour

immersion but without an applied cathodic polarization (solution 6) the IZI values obtained were marginally higher than that obtained in same solution with applied cathodic polarization, and in the uninhibited solution (solution 2) with cathodic polarization. Though marginal, these observations suggest that the inhibitive effects on CFRP degradation due to of SDS adsorption is sustained both in the presence and absence of a cathodic polarization. Comparing the sustained and higher IZI values obtained both after testing under cathodic polarization in inhibited solution (solution 7) and after washing in distilled water and testing in uninhibited solution after 1 hour immersion under cathodic polarization (solution 8) with values obtained in uninhibited solution under cathodic polarization (solution 2) confirms the stability of the inhibitive effect, and hence the adsorbed layer obtained on CFRP by immersion of CFRP in SDS containing solution with or without cathodic polarization.

The acquired impedance spectra were fitted to the equivalents circuits presented in **Fig. 4d** (circuits 1 and 2). The one time constant equivalent circuit (**Fig. 4d,** circuit 1) was used to fit data obtained in the absence of SDS in 50 mM NaCl with or without cathodic polarization, while the two time constant equivalent circuit (**Fig. 4d,** circuit 2) was used to fit data acquired in the presence of SDS and the results presented in **Fig 5**. From **Fig. 5a**, it is observed that irrespective of the testing sequence, with application of cathodic polarization and without application of a cathodic polarization, once the CFRP has been exposed to SDS containing solution the measured values of the charge transfer resistance (R_{ct}) was consistently higher than the polarization resistance (R_p) measured in uninhibited solution with cathodic polarization (solution 2). This observation is indicative of an increased and sustained resistance to charge transfer and /or mass transfer processes after exposure of CFRP to SDS laden solutions. The resistance attributed to the adsorbed SDS layer (R_{ads}) is observed to be lowest in the absence of a cathodic polarization (solutions 3 and 4) but increased markedly in the presence of SDS and cathodic polarization or after prior simultaneous exposure to both. By comparison of the R_{ads} values in solution 4 (CFRP exposure to SDS at OCP and then measurement in 50 mM NaCl only) and in solution 8 (CFRP exposure to SDS at -1000 mV_{SCE} and them measurement in 50 mM NaCl at -1000 mV_{SCE}) which are similar, it is concluded that the adsorption of SDS on CFRP surface and the resultant inhibitive effect is sustained, with or without the simultaneous application of a cathodic polarization. From **Fig. 5b**, a drastic reduction in the double layer capacitance (C_{dl}) is observed in SDS containing test media without cathodic polarization (solution 3) and was sustained after washing in distilled water and testing in 50 mM NaCl after 1 hour immersion

without cathodic polarization (solution 4). This same trend of marked decrease of double layer capacitance (C_{dl}) is observed in all the other sequential tests involving CFRP exposure to SDS with/or after application of cathodic polarization of -1000 mV_{SCE} (solutions 5,6,7, and 8). The capacitances in all the respective sequential tests were observed to be dominated by capacitive effects attributed to the adsorbed SDS layer which is an additional confirmation of the presence of a persistent adsorbed layer on CFRP surface after exposure to SDS containing solutions with or without an applied cathodic polarization.

3.2. Results from surface analysis of CFRP surface

A very plausible mode of SDS interaction with the surfaces of the electrochemically active carbon fibres is by adsorption. The adsorption of surfactants on metal surfaces have been known to influence electrochemical behaviour **[81]**, with positive implications for corrosion mitigation and electroplating **[82]**. The presentations of micelles observed in SDS bulk solutions is reported **[83]** to vary with SDS concentration. In bulk solution, SDS forms roughly spherical micelles at SDS concentration of 8 mM **[83]**, elliptical micelles at 80 mM SDS concentration **[84]**,and some proof of cylindrical micelles at 0.87 M **[85]**. At the interface between the bulk solution containing SDS and a substrate (in this case carbon fibres), there is bound to be some changes in the nature of the aggregation on the substrate. Király et al. **[86]** studied the organization of sodium n-decyl sulfate at the graphite/solution interface by adsorption calorimetry and reported that adsorption of SDeS from aqueous solution onto graphite follows a two-step mechanism as a function of the surfactant concentration. The first step at low concentrations involving a strongly exothermic process that is apparently independent of (or only marginally dependent on) the temperature and the surface coverage, and results in the formation of a flat, ordered monolayer. The second adsorption step was postulated to be less exothermic, and apparently independent of (or only marginally dependent on) the surface coverage, but strongly dependent on the temperature. To explain their results **[86]** a mechanism in which two adsorbed phases (a water-rich and a surfactant-rich domains) coexist during monolayer formation in the first step was proposed with the formation of loosely packed surface hemi-cylinders in the second step facilitates by the prior formed underlying monolayer as the solution concentration is increased towards the critical micelle concentration (cmc) . With calorimetric evidence that the adsorption and aggregation of cationic and anionic surfactants follow the same adsorption mechanism on the surface of

graphite, they [86] concluded that the similarities in the aggregation behaviours of SDeS in aqueous solution and at the graphite/solution interface originated from intermolecular hydrophobic interactions. Manne at al. [87,88] employed atomic force microscopy to image adsorbed surfactant aggregates on graphite surface, presented an unambiguous experimental proof of the formation of hemi-cylindrical micelles on graphite by surfactants, and attributed the hemi-micelle structure to templating by the epitaxially bound monolayer. Wanless and Ducker [89] studied the organization of sodium dodecyl sulphate at the graphite-solution interface and reported that sodium dodecyl sulfate adsorbed to graphite in an organized structure in the form of hemi-cylindrical periodic structures (aggregates of height ≈ 1.7 ± 0.7 nm) when the solution concentration exceeded 2.8 mM (up to 81 mM) but observed no structures at or less than 1.6 mM SDS concentration. They [89] showed the variation of the distance between the adsorbed hemi-cylindrical aggregates with both surfactant concentration and ionic strength, and reported that the periodicity of the structures decreased with increasing SDS concentration. On the basis of these observations they [89] postulated that the surface aggregation concentration (sac) is in the range of 1.6 to 2.8 mM which is about a quarter of the critical micelle concentration (cmc). The surface aggregation concentration (sac) is reported to be sensitive to the presence of NaCl (equivalent to changes in ionic strength); decreasing in value in the presence of NaCl. In a follow-up work [83], Wanless and Drucker established the weak influence of divalent ions on anionic surfactant surface-aggregation, which can explain the challenges observed in attempts at exploiting the reduced cathodic activity on CFRP achieved in this work in mitigating multi-material corrosion in assemblies comprised of CFRP and metals whose anodic dissolution in the presence of SDS is prone to serve as sources of divalent and/or trivalent ions [78].

Domínguez [90] employed molecular dynamics simulations to study adsorption of sodium dodecyl sulfate (SDS) molecules onto graphite surface in different salt (NaCl)/water solutions and obtained results showing the formation of hemicylindrical aggregates, at different salt concentrations in agreement with AFM data [89], but with the hemicylinders exhibiting different structures as the salt concentration was increased. There is a consensus that surfactants on hydrophobic surfaces (e.g., graphite) self-organize in hemicylinders due to the fact that the substrates interact primarily with the tail groups through van der Waals forces [87], while hydrophilic substrates interact primarily with the surfactant headgroups giving rise to different presentation of aggregates on hydrophilic surfaces.

To determine the possible origins of the observed electrochemical effects on CFRP after treatment with SDS surface analyses were made employing combining scanning electron microscopy with energy dispersive x-ray (EDX) elemental mapping of CFRP surface prior and post exposure and the results presented in **Figs. 6** and **7**.

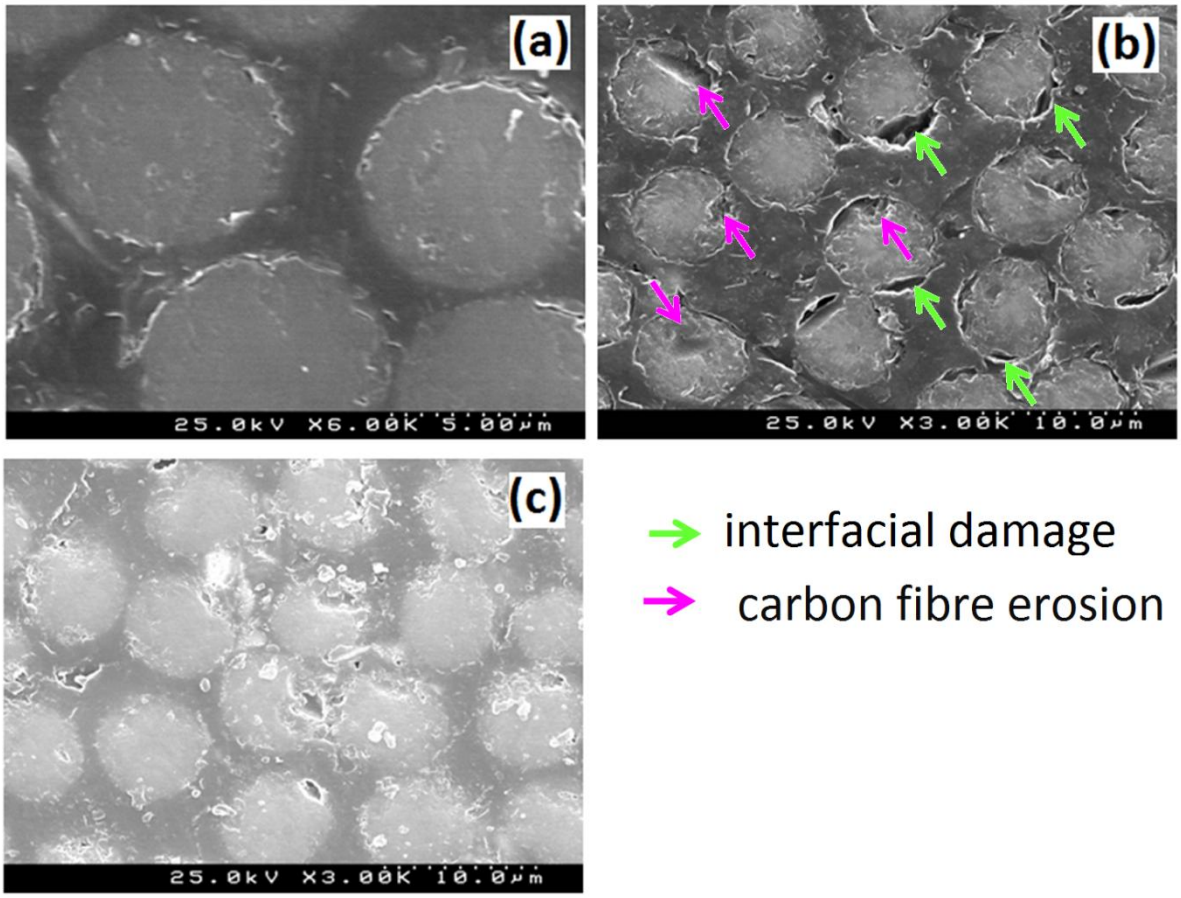

Fig. 6. SEM images of CFRP as received (a),and after immersion in 50 mM NaCl for 2 hours at -1000 mV_{SCE} in the absence (b), and presence of 5 mM SDS (c).

SEM images of CFRP (**Fig.6.**) before and after exposure to cathodic polarizations of -1000 mV_{SCE} in the absence (**Fig.6b**) and presence of SDS (**Fig.6c**) show marked reduction of the interfacial damage observed under similar polarization in its absence. On application of a cathodic polarization without SDS (**Fig.6b**) composite degradation manifest predominantly as interfacial damage (indicated with lemon green arrows) and carbon fibre erosion (indicated with magenta arrows). Both of these two degradation mechanisms result in increase in surface area which in turn leads to increase in electrochemical activity. In contrast, on application of a cathodic polarization in the presence of SDS (**Fig.6c**) composite degradation by both mechanisms; interfacial damage and carbon fibre erosion is mitigated. This effect is inferred to emanate from the presence of an adsorbed layer of SDS on the composite surface that interferes with the

degradative electrochemical processes that can take place on CFRP surface under cathodic polarization **[71,91-93]**.

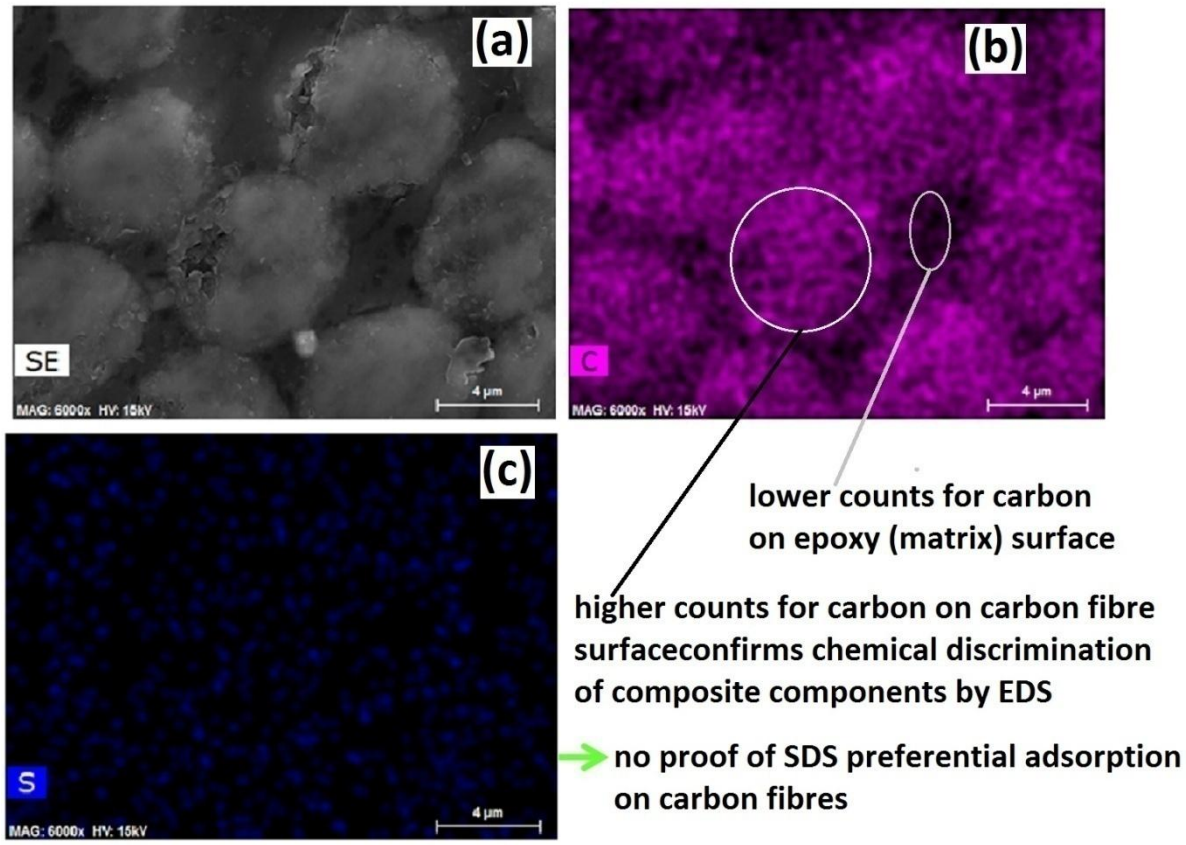

Fig. 7. EDX mapping for carbon and sulphur on CFRP surface post treatment in SDS and washing in distilled water.

The EDX mapping results for carbon (**Fig. 7b**) resolves the spatial distribution of the carbon fibres on the CFRP surface by the higher counts recorded for carbon over carbon fibre surfaces in the composite compared to the epoxy matrix. On the contrary, the EDX mapping results for sulphur which was used as a marker for the presence of SDS only confirmed the presence of SDS on CFRP surface post exposure but was unable to confirm any preferential adsorption/interaction with the carbon fibres or epoxy matrix. This is thought to arise from the small amount of SDS on the sample surface. Confocal Raman spectroscopy/microscopy was employed in an attempt to overcome this challenge, and the results presented in **Figs. 8.** and **9**.

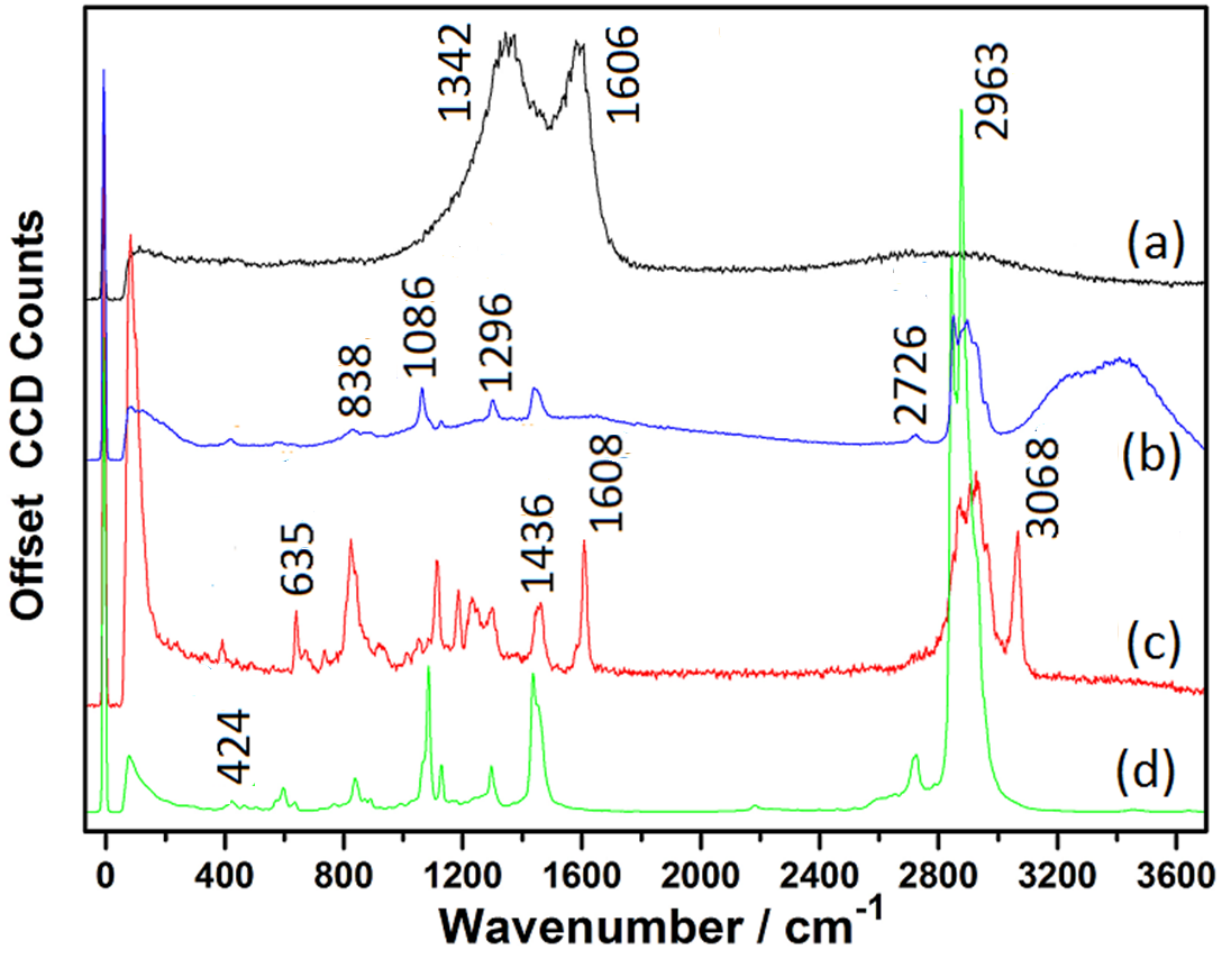

Fig. 8. Raman Spectra measured (a) over carbon fibres in CFRP as is, (b) in saturated SDS solution (c) over carbon fibres in CFRP after 1 hr in 50 mM NaCl + 10 mM SDS solution at -1000 mV_{SCE}, , and (d) on SDS powder.

True to type the Raman spectra of the long chain sodium dodecyl sulphate (SDS) (**Table 1**, **Fig. 8**, spectra (b) and (d)) is marked by peaks attributable to skeletal vibration modes of the linear tail. Vibration in the higher energy regions of the spectra between 2800 cm^{-1} and 3000 cm^{-1} has been generally attributed to C-H stretching vibrations and dominated by two peaks around 2850 cm^{-1} and 2885 cm^{-1} linked to the symmetric and anti-symmetric vibration modes of the CH_2 groups of the tail, respectively **[94-97]**. Peaks in the lower energy region in the range of 1050 to 1500 cm^{-1} were attributed to skeletal vibration modes predominantly comprised of C-C stretching vibrations between 1050 cm^{-1} and 1150 cm^{-1}, CH_2 twisting mode around 1300 cm^{-1}, and the CH_2 bending modes around 1440-1460 cm^{-1} **[94,95]**. The bands between 400 cm^{-1} and 1000 cm^{-1} have been generally attributed to the $OSO_3^-Na^+$ polar headgroups **[94,95],** and the bands in the solid SDS around 406 cm^{-1},425 cm^{-1},573 cm^{-1},598 cm^{-1}, and 635 cm^{-1} closely attributed to the SO_3^- moiety **[95]** and band around 841 cm^{-1} and 1000 cm^{-1} attributed to S-OC headgroup vibrations **[94,95]**.

According to Johnson and Tyrode **[98]** disagreements exist in literature on the assignment of Raman peaks of SDS around 1060 cm^{-1} and 1088 cm^{-1} (in the 1000 cm^{-1} and 1100 cm^{-1} range) in adsorption experiments. Whereas Kalyanasundaram and Thomas **[99]** attributed the peaks reported at 1064 cm^{-1} and 1086 cm^{-1} to C–C stretch and vs(SO_3) respectively, Picquart **[94]** in a later study attributed the peak observed at 1063 cm^{-1} to a superposition of a skeletal C–C stretch and vs(SO_3). This latter assignment and explanation for the peak at 1063 cm^{-1} by Picquart, **[94]** is supported by the works of two independent authors **[99,100]** who using other molecules possessing either C–C bonds or an SO_3 group, but not both, confirmed that the superposition of both a C–C stretch and vs(SO3) manifest resonances around 1063 cm^{-1} **[98]**. In the light of these, the peak assignments of Picquart **[94]** are adopted in this work for monitoring SDS interaction/adsorption on CFRP surface.

The emergence of peaks in the range 400 to 1000 (Table 1) that is non-controversially attributed to SDS headgroup bands around 406 cm^{-1},425 cm^{-1},573 cm^{-1},598 cm^{-1}, and 635 cm^{-1} particularly attributed to the SO_3^- moiety **[95]** and bands around 841 cm^{-1} and 1000 cm^{-1} attributed to S-OC headgroup vibrations **[94,95]** on carbon fibres after immersion in 50 mM NaCl + 10 mM SDS solution at -1000 mV_{SCE} (**Fig. 8**, spectra (c)) confirm interaction/adsorption of sodium dodecyl sulphate (SDS) onto carbon fibre surface. The well defined nature and sharpness of the peaks in the 1050 - 1150 cm^{-1} region attributable **[95]** to skeletal vibrations (C-C binding) on carbon fibre surface, after immersion in very dilute SDS solution under cathodic polarization (**Fig. 8**, spectra (c)) compared to CCD counts in saturated SDS solution (**Fig. 8**, spectra (b)), and SDS powder (**Fig. 8**, spectra (d)) is suggestive of some ordered arrangement of SDS molecules on carbon fibres under the test conditions, that does not appear to constrain these skeletal (C-C binding) vibrations; possibly hemi-micellar aggregates **[98]**.

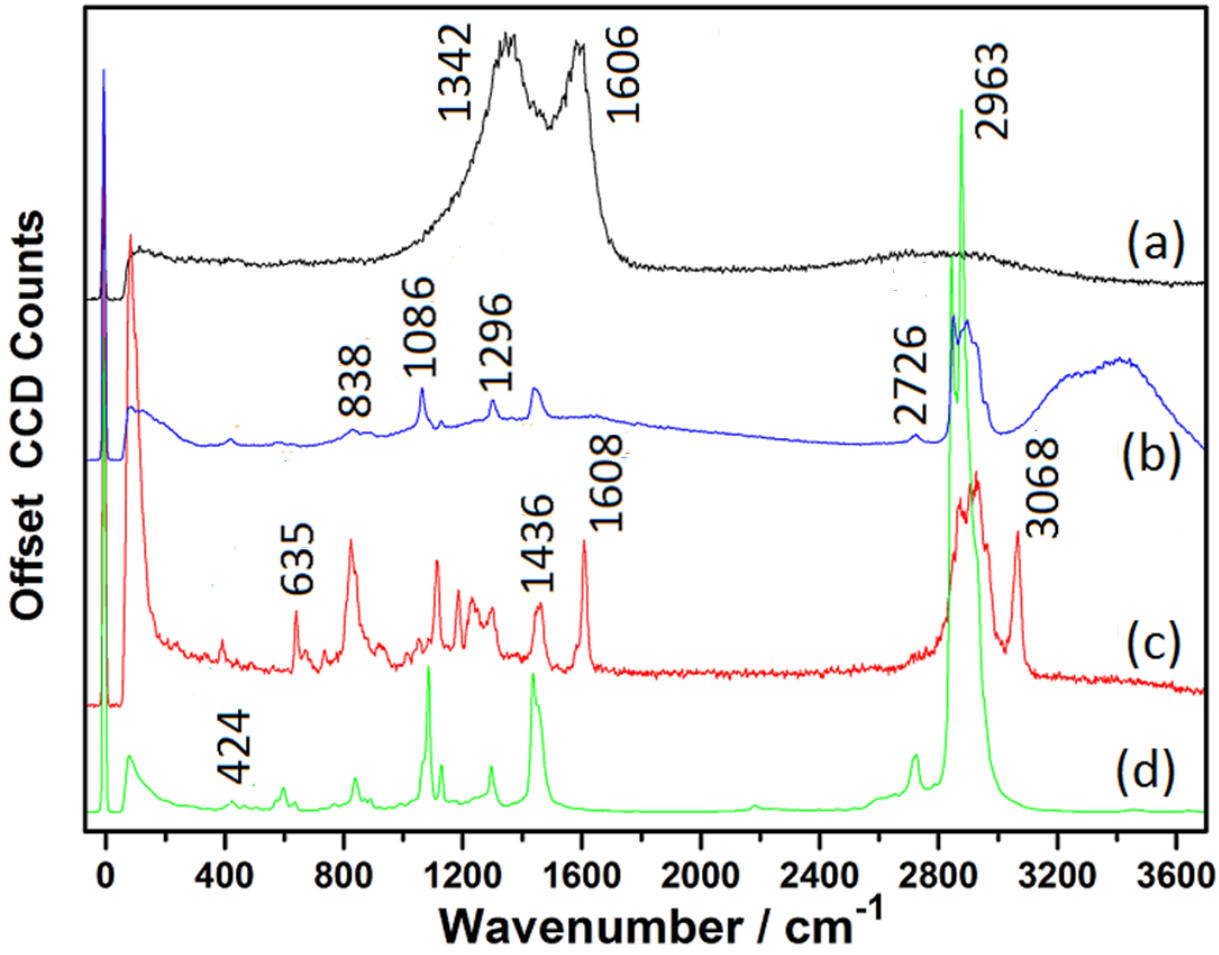

Fig. 8. Raman Spectra measured (a) over carbon fibres in CFRP as is, (b) in saturated SDS solution (c) over carbon fibres in CFRP after 1 hr in 50 mM NaCl + 10 mM SDS solution at -1000 mV_{SCE}, , and (d) on SDS powder.

Although the Raman spectra acquired over the epoxy component of the CFRP composite (**Fig. 9**, spectra (a and b)) presents bands for epoxy that are difficult to distinguish from those of SDS (**Fig. 9**, spectra (c and d))particularly in the 1000 to 3200 cm^{-1} range, it is possible to establish the presence of SDS on the surface of the epoxy matrix from the peaks in the range of 400 cm^{-1} to 1000 cm^{-1} generally attributed to the headgroup vibrations. Proof of SDS presence on the epoxy matrix surface is established by the observance of enhanced peaks around 392 cm^{-1}, 580 cm^{-1}, and 821 cm^{-1}. Okabayashi et al., **[101]** have reported a medium peak around 417-420 cm^{-1} they attributed to $-SO_3$ rocking vibrations, medium peak around 580-584 cm^{-1} attributed to $-SO_3$ symmetric deformation, and a very sharp peak around 1062-1065 cm^{-1} they attributed to $-SO_3$ symmetric stretching vibrations.

On the basis of the observed data trends in this work and various literature reports on SDS

458 adsorption on graphite surface **[94,95,98,99,101,102]**, it is postulated that SDS adsorbs to both
459 the carbon fibres and epoxy matrix components of the CFRP composite albeit by different
460 mechanisms with monolayer adsorption predominant on the epoxy matrix and hemicelle
461 formation predominating on carbon fibre surface (**Fig. 10**). This postulation is supported by the
462 results of in-situ AFM studies carried out on highly ordered pyrolytic graphite (HOPG) samples
463 exposed to 50 mM NaCl solutions containing different concentrations of SDS and presented
464 below (in Section 3.3 and **Figs. 11** to **13**).
465
466
467
468
469
470
471
472
473
474
475
476
477
478
479
480
481
482
483
484
485
486
487
488
489

Table 1: Table of observed Raman peaks.

Peak No.	SDS Powder	Saturated SDS Solution	CFRP after -1 V in SDS	Carbon fibres as is	Epoxy of CFRP as is	Epoxy of CFRP after -1 V in SDS
1.	424.12	211.19	240.27	1342.46	505.81	243.17
2.	595.81	415.59	392.80	1605.97	747.59	392.80
3.	634.73*	832.16	640.28*		802.20	580.22
4.	837.58	1062.08	670.72		832.10	821.31
5.	1085.78	1298.63**	824.03		1001.30	929.18
6.	1127.74	1440.87**	1112.03		1109.60	1001.21
7.	1296.07*	2724.39	1185.10		1185.35	1187.70
8.	1435.83*	2849.04	1231.73		1316.91	1342.07
9.	2726.52	2897.05	1249.80		1446.38	1387.82
10.	2844.85	2957.14**	**1298.63*/****		1558.92	1455.96
11.	2876.21*		**1450.94*/****		1603.50	1605.36
12.			1460.99		2546.74	2543.19
13.			1607.83		2601.16	2760.53
14.			2874.13*		2653.03	2926.12
15.			2884.56		2710.95	2967.45
16.			2905.37		2759.93	3061.60
17.			2926.12		2819.12	3118.30
18.			2932.33		2929.85	
19.			2957.14**		3067.44	
20.			2963.32			
21.			3067.69			

*Peaks observed around this wavenumber in SDS or SDS solutions

** Peaks observed around this wavenumber in CFRP and SDS powder or solutions

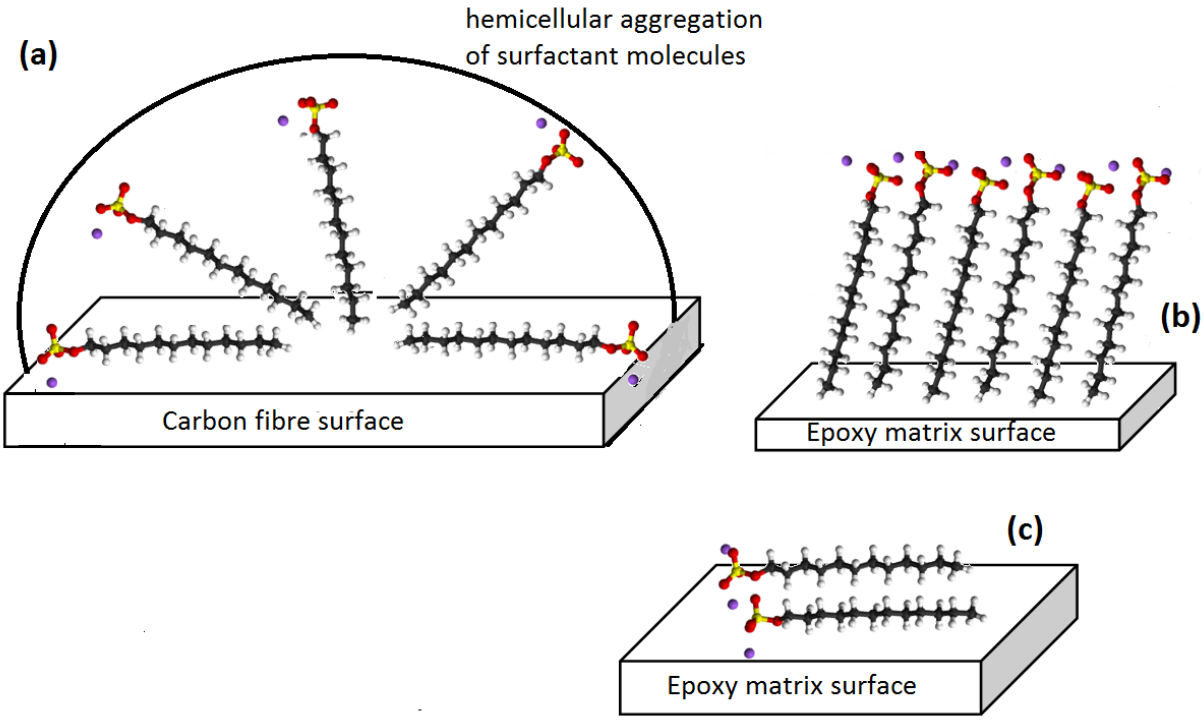

Fig. 10. Proposed mechanisms of SDS adsorption onto carbon fibre and epoxy matrix surfaces (For clarity more of the SDS molecules forming the hemi-cellular aggregate(s) in Fig. 10a were omitted).

3.3. Results from AFM surface analysis of Carbon (Highly Ordered Pyrolytic Graphite) surface prior to and after exposure to 50 mM NaCl solutions containing SDS.

Due to challenges to obtaining atomically flat surfaces of the CFRP composite, and in the light of the fact that SDS interaction with CFRP most probably occur predominantly via the component carbon fibres, AFM studies were conducted using highly ordered pyrolytic graphite (HOPG) samples exposed to 50 mM NaCl solutions containing different concentrations of SDS (0 -20 mM SDS) with and without cathodic polarization.

Results from AFM measurements on HOPG surfaces after exposure to 50 mM NaCl solutions containing SDS (**Figs. 11** and **12**) confirm interaction of SDS with carbon surface evidenced by a periodicity with a pitch size of ≈ 4.7 nm in 50 mM NaCl + 5 mM SDS (**Fig.11**). and ≈ 4.1 nm in 50 mM NaCl + 10 mM SDS (**Fig.12**). Such concentration dependent variations in the periodicity of adsorbed layers have been reported in the literature **[89]**. The periodicity trend observed in this work is in tandem with recent literature data on the periodicity of cylinders obtained in SDS solutions on HOPG **[103]** which reported that the micellar spacing varies with

515 respect to the SDS concentration, decreasing from a periodicity of 6.7 ± 0.1 nm at 7.5 mM SDS
516 to 4.5 ± 0.1 nm at 15 mM SDS and a slight increase in the micellar periodicity from 4.5 ± 0.1 nm
517 to 4.8 ± 0.1 nm on addition of 20 mM NaCl. A much earlier work **[89]** had reported periodicities
518 of 5.2 nm in 81 mM SDS solutions, ≈ 5 nm in 16 mM SDS in NaCl solutions, and 5.2 - 6.5nm in 2.8
519 mM SDS solutions in the presence of NaCl. Discrepancies in estimations of periodicity of micellar
520 semi cylinders on HOPG can be attributed to a variety of factors such as the possible presence of
521 contamination by the SDS hydrolysis product; 1-dodecanol **[89]**, differences/changes in the ionic
522 strength of solution, temperature, scanner etc.
523

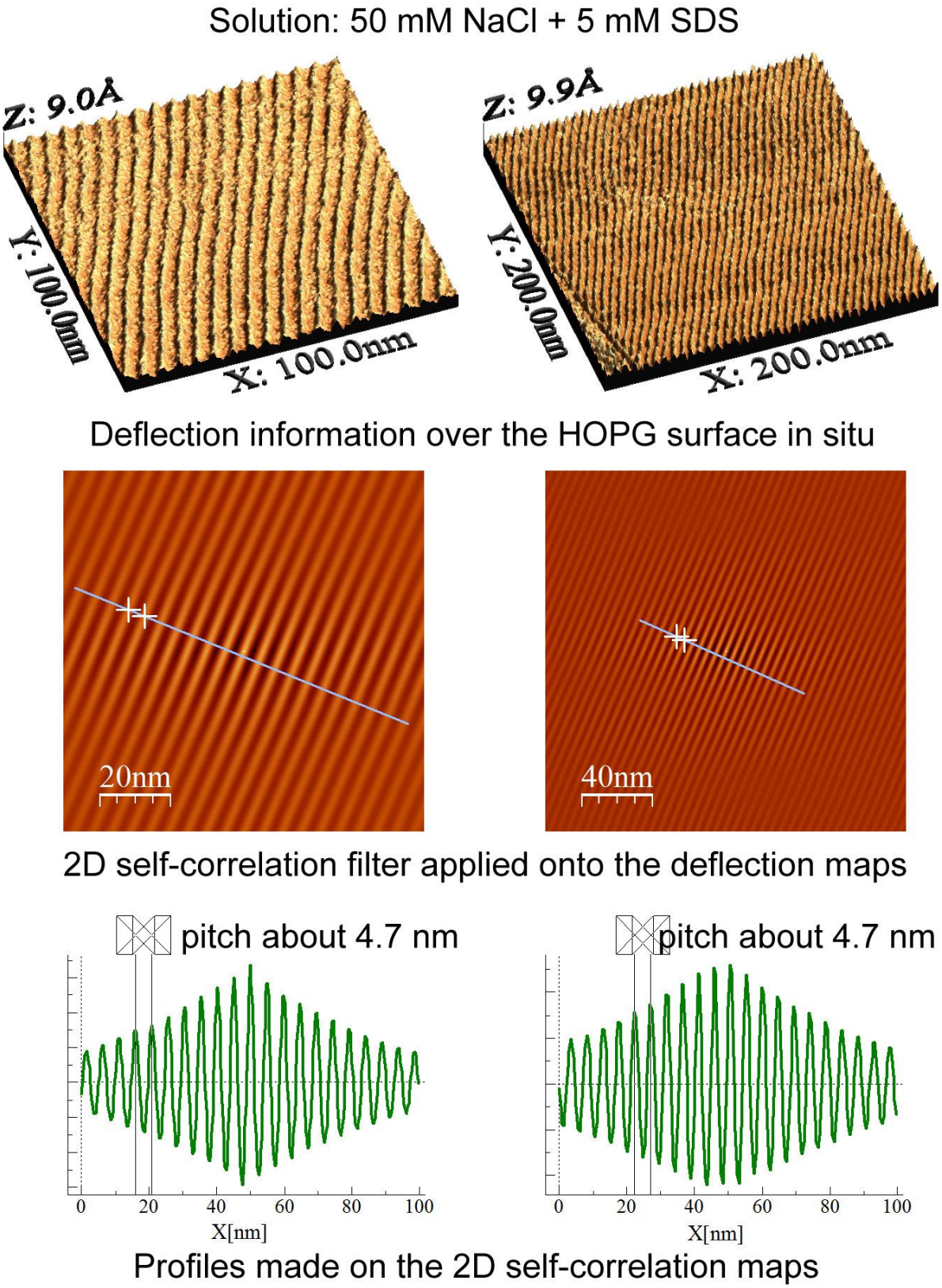

Fig. 11. Atomic force microscopy data acquired on HOPG sample in 50 mM NaCl + 5 mM SDS solution.

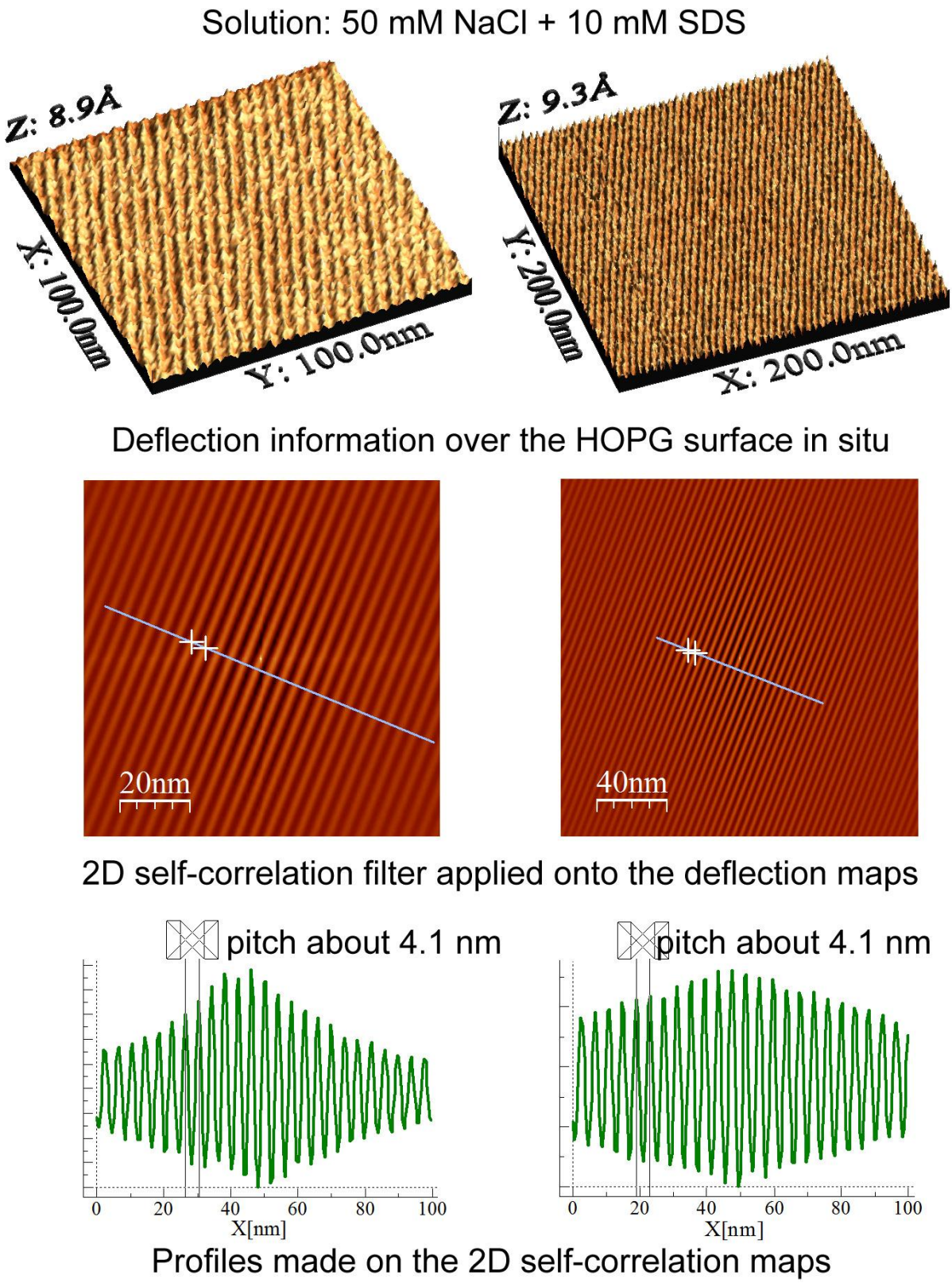

529

530 Fig. 12. Atomic force microscopy data acquired on HOPG sample in 50 mM NaCl + 10 mM SDS
531 solution.

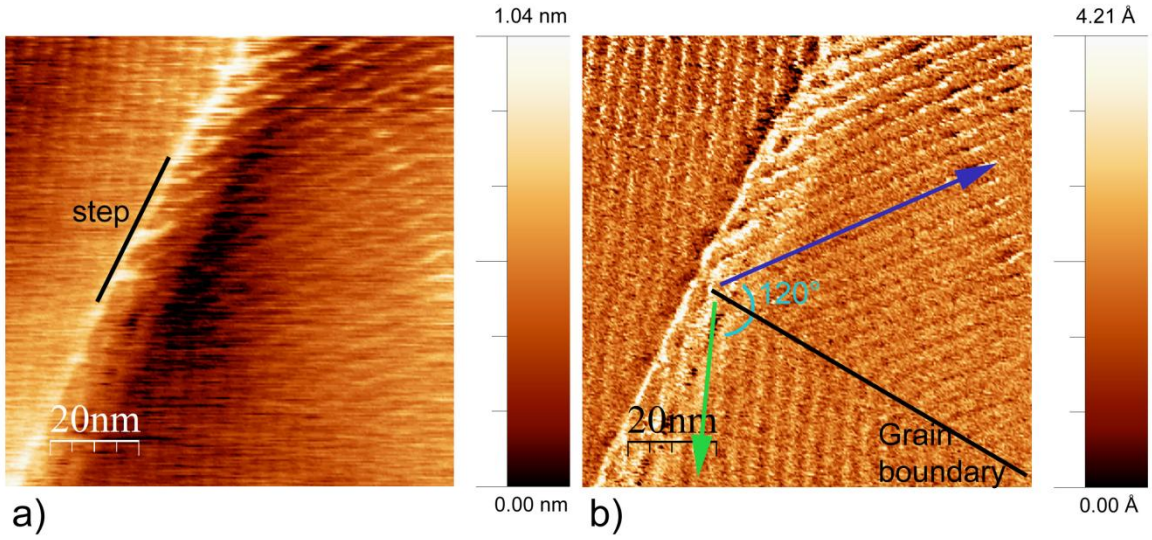

Fig. 13. AFM topography (a) and Deflection (b) information over the HOPG surface in-situ in 50 mM NaCl + 10 mM SDS solution (On this image it can be observed that the half cylinders are aligned in different directions.

From Fig. 13; ((a) the AFM topography and (b) deflection images) acquired over the HOPG surface in-situ in 50 mM NaCl + 10 mM SDS solution it can be observed that the half cylinders of the SDS "molecular aggregations" align in different directions forming "boundaries". The presence of a majority of these boundaries have been attributed to steps in the graphite surface, but in the light of the fact that not every step contained a grain boundary, and not every boundary was located at a step **[89]**, these differences in orientation have also been associated with the underlying hexagonal structure of the graphite **[87]**. An alternative explanation was that the orientation may be due to growth from steps on the graphite, while the step orientation is determined by crystallography of the carbon surface **[87,89]**.

Chen et al., **[104]** have demonstrated that the electrical state of a surface (namely surface charge or applied potential) plays an integral role in determining the morphology of surfactants at solid interfaces and thus the electrical parameter can be easily manipulated in situ, as a tunable means to control films of soft condensed matter. Chen et al., **[104]** also demonstrated that the surface concentrations of three surfactants; sodium dodecyl sulfate (SDS), N-dodecyl-N,N-dimethyl-3-ammonio-1-propanesulfonate (DDAPS) and N-decyl-N,N,N-

556 trimethylammonium triflate (DeTATf), adsorbed on Au (111) electrode surface were lowest at
557 cathodic potentials (which corresponds to negative charge densities at the electrode
558 surface),and hence rightly postulated that positive charge(s) on the metal surface is needed to
559 screen the electrostatic repulsion between the surfactant head-groups allowing for a much
560 greater packing density.

561 Based on insights drawn from literature **[104]** cathodic polarization of carbon surface(s)
562 in the presence of SDS was anticipated to lead to a decrease in adsorption of molecules as
563 observed for Au substrate **[104]**. Since PZC on HOPG is about -0.24 V_{SCE} **[29, 104,105,106,107]**
564 the surface will be negatively charged at cathodic polarizations below that potential. This
565 change will most probably result in collapsing of the semi-cylindrical structure of SDS adsorbed
566 on HOPG surface without polarization. Such anticipated scenario of reduced SDS adsorption on
567 carbon surface under cathodic polarization appear to be at variance with electrochemical test
568 data, which might be indicative that some effects not related to increase in SDS adsorption unto
569 carbon surface at cathodic polarization(s) are most probably responsible for the observed
570 reduction in cathodic activity of CFRP on exposure to SDS containing solutions.

571 Efforts to confirm these expectations by making in-situ AFM measurements on HOPG
572 surface in the presence of SDS containing solutions with applied cathodic polarization were
573 unsuccessful at the moment due to the problems of disengagement of the surface by the tip on
574 application of polarization and gas evolution in a cell with small electrodes and little space that
575 makes flushing the gas challenging.

576 Tip disengagement occurred during attempts to measure surface topography of HOPG
577 simultaneously with application of a DC voltage. The challenge of tip disengagement is not
578 trivial and can be the subject of further study. However, an appreciation of this challenge is vital
579 to its resolution. First of all by applying a potential difference (positive or negative) between
580 HOPG and a counter electrode (Pt) an electrostatic force develops between the sample and a
581 tip. We suspect that the force or thermal drift due to current passing through the solution may
582 push or pull the tip from/to the surface as the deflection signal changes and goes out of the
583 limits (+/-10 V). This does not let us to stay in the "repulsive force regime" in which we make
584 measurements of distribution of surfactant micelles on the surface. FurthermoreB, the applied
585 potential difference being rather high (-1000 mV) promote side electrochemical reactions
586 where water is split with the formation of gas(es); either H_2 or O_2. The gas bubbles then blocked
587 the path through which laser beam was directed onto the cantilever and eventually obstructed

588 the measurements in the closed glass fluid cell.

589 In order to solve the problem, perhaps a much lower potential difference has to be
590 applied compared to what was used in amperometric and EIS measurements in this work. Using
591 a lower potential difference will put us away from real experimental conditions, though it may
592 allow to perform AFM experiments in electrostatic repulsive force regime. Gas evolution is a
593 more significant problem which calls for development of an open liquid cell to drain gas bubbles
594 away. However, there is noticeable evaporation of electrolyte solution in an open fluid cell,
595 which has to be solved as well. We should also mention that there must be a certain thermal
596 equilibrium achieved between the solution and the cantilever. This is important as the drift of
597 deflection signal appears to be too fast when there is no thermal equilibrium between the
598 cantilever and the solution. The high changes of cantilever's deflection are especially noticed
599 when a fresh solution is pumped to the fluid cell. At high drift it is impossible to put a setpoint
600 necessary to maintain the repulsive force regime. Hence some time has to be given to bring the
601 cell to some sort of stationary conditions before any attempts to run a AFM experiment. Again
602 different factors have to be solved simultaneously when performing DC polarization
603 simultaneously with AFM measurements such as electrostatic force acting on tip, thermal drift,
604 gas evolution and with that many factors we have not yet been able to obtain meaningful
605 results.

606

607 **4. Conclusions**

608 From the results it is concluded that SDS interacts with CFRP surface resulting the
609 formation of a persistent adsorbed layer. Electrochemical tests demonstrate that adsorption of
610 SDS to CFRP surface leads to reduced electrochemical activity evidenced by a reduction in its
611 ability to sustain cathodic reactions. Surface analysis by confocal Raman spectroscopy of the
612 treated CFRP surfaces post-treatment indicates adsorption of sodium dodecyl sulphate on both
613 the surfaces of the reinforcing carbon fibres and the epoxy matrix of the composite. Surface
614 analysis by scanning electron microscopy confirm mitigation of the CFRP composite degradation
615 under impressed cathodic polarization in the presence of SDS or after prior exposure to SDS
616 containing solution.

Acknowledgements

Funding from FCT project: "Corrosion and Corrosion Protection in Multi-material Systems", (PTDC/CTM/108446/2008), and European FP7 project: "Active PROtection of multi-material assemblies for AIRcrafts" ["PROAIR" (PIAPP-GA-2013-612415)] are acknowledged. S.U. Ofoegbu and S. Kallip acknowledges Fundação para a Ciência e a Tecnologia (FCT) Portugal for doctoral (SFRH/BD/75167/2010) and post-doctoral (SFRH/BPD/64580/2009) grants respectively. This work was developed within the scope of the project CICECO-Aveiro Institute of Materials, POCI-01-0145-FEDER-007679 (FCT Ref. UID /CTM /50011/2013), financed by national funds through the FCT/MEC and when appropriate co-financed by FEDER under the PT2020 Partnership Agreement.

Conflict of Interests: The authors declare that there are no conflict of interests.

References

1. Elving, P. J., & Krivis, A. F. (1958). Voltammetric studies with graphite indicating electrode. Analytical Chemistry, 30(10), 1645-1648.

2. Lord Jr, S. S., & Rogers, L. B. (1954). Polarographic studies with gold, graphite, and platinum electrodes. Analytical Chemistry, 26(2), 284-295.

3. Gaylor, V. F., Conrad, A. L., & Landerl, J. H. (1957). Use of wax-impregnated graphite electrode in polarography. Analytical Chemistry, 29(2), 224-228.

4. Gaylor, V. F., Conrad, A. L., & Landerl, J. H. (1957). Polargraphic Determination of Antioxidants in Gasoline. Analytical Chemistry, 29(2), 228-232.

5. Adams, R. (1958). Carbon paste electrodes. Analytical Chemistry, 30(9), 1576-1576.

6. Morris, J. B., & Schempf, J. M. (1959). Voltammetric Studies at Graphite Electrode. Analytical Chemistry, 31(2), 286-291.

7. Miller, F. J., & Zittel, H. E. (1963). Fabrication and Use of Pyrolytic Graphite Electrode for Voltammetry in Aqueous Solutions. Analytical Chemistry, 35(12), 1866-1869.

8. Beilby, A. L., Brooks Jr, W., & Lawrence, G. L. (1964). Comparison of the Pyrolytic Carbon Film Electrode with the Wax-Impregnated Graphite Electrode. Analytical Chemistry, 36(1), 22-26.

9. Brezina, M. (1966). Estimation of electrochemical activity of carbon using a paste electrode. Nature, 212, 283.

10. Noel, M., & Anantharaman, P. N. (1986). Voltammetric studies on glassy carbon electrodes I: Electrochemical behaviour of glassy carbon electrodes in H_2SO_4, Na_2SO_4 and NaOH media. Surface and Coatings Technology, *28*(2), 161-179.

11. Taylor, R. J., & Humffray, A. A. (1973). Electrochemical studies on glassy carbon electrodes: I. Electron transfer kinetics. Journal of Electroanalytical Chemistry and Interfacial Electrochemistry, 42(3), 347-354.

12. Kostecki, R., Jeong, S. K., Lei, J., Song, X., Zhuang, V., Striebel, K., & McLarnon, F. Electrochemical Degradation of Carbon in Composite Cathodes for Li-ion Cells.

13. Li, H., & Zhou, H. (2012). Enhancing the performances of Li-ion batteries by carbon-coating: present and future. Chemical Communications, 48(9), 1201-1217.

14. Hong, J. K., Lee, J. H., & Oh, S. M. (2002). Effect of carbon additive on electrochemical performance of LiCoO 2 composite cathodes. Journal of power sources, 111(1), 90-96.

15. Thorat, I. V., Mathur, V., Harb, J. N., & Wheeler, D. R. (2006). Performance of carbon-fiber-

containing LiFePO 4 cathodes for high-power applications. Journal of power sources, 162(1), 673-678.

16. Trogadas, P., Fuller, T. F., & Strasser, P. (2014). Carbon as catalyst and support for electrochemical energy conversion. Carbon, 75, 5-42.

17. Rodriguez, N. M., Kim, M. S., & Baker, R. T. K. (1994). Carbon nanofibers: a unique catalyst support medium. The journal of physical chemistry, 98(50), 13108-13111.

18. Uchida, M., Fukuoka, Y., Sugawara, Y., Eda, N., & Ohta, A. (1996). Effects of Microstructure of Carbon Support in the Catalyst Layer on the Performance of Polymer-Electrolyte Fuel Cells. Journal of The Electrochemical Society, 143(7), 2245-2252.

19. Roen, L. M., Paik, C. H., & Jarvi, T. D. (2004). Electrocatalytic corrosion of carbon support in PEMFC cathodes. Electrochemical and Solid-State Letters, 7(1), A19-A22.

20. Qu, D. (2007). Investigation of oxygen reduction on activated carbon electrodes in alkaline solution. Carbon, 45(6), 1296-1301.

21. Ma, Y., Zhao, J., Zhang, L., Zhao, Y., Fan, Q., Hu, Z., & Huang, W. (2011). The production of carbon microtubes by the carbonization of catkins and their use in the oxygen reduction reaction. Carbon, 49(15), 5292-5297.

22. Wei, W., Tao, Y., Lv, W., Su, F.Y., Ke, L., Li, J., Wang, D.W., Li, B., Kang, F. and Yang, Q.H. (2014). Unusual high oxygen reduction performance in all-carbon electrocatalysts. Scientific reports, 4.

23. Šljukić, B., Banks, C. E., Mentus, S., & Compton, R. G. (2004). Modification of carbon electrodes for oxygen reduction and hydrogen peroxide formation: The search for stable and efficient sonoelectrocatalysts. Physical Chemistry Chemical Physics, 6(5), 992-997.

24. Šljukić, B., Banks, C. E., & Compton, R. G. (2005). Exploration of stable sonoelectrocatalysis for the electrochemical reduction of oxygen. Electroanalysis, 17(12), 1025-1034.

25. Chu, X., & Kinoshita, K. (1997). Surface modification of carbons for enhanced electrochemical activity. Materials Science and Engineering: B, 49(1), 53-60.

26. Cline, K. K., McDermott, M. T., & McCreery, R. L. (1994). Anomalously slow electron transfer at ordered graphite electrodes: influence of electronic factors and reactive sites. The Journal of Physical Chemistry, 98(20), 5314-5319.

27. Banks, C. E., Davies, T. J., Wildgoose, G. G., & Compton, R. G. (2005). Electrocatalysis at graphite and carbon nanotube modified electrodes: edge-plane sites and tube ends are the reactive sites. Chemical Communications, (7), 829-841.

28. McCreery, R. L., & McDermott, M. T. (2012). Comment on electrochemical kinetics at ordered graphite electrodes. Analytical chemistry, 84(5), 2602-2605.

29. Kneten, K.R. and McCreery, R.L., 1992. Effects of redox system structure on electron-transfer kinetics at ordered graphite and glassy carbon electrodes. Analytical Chemistry, 64(21), pp.2518-2524.

30. Banks, C.E. and Compton, R.G., (2005). Exploring the electrocatalytic sites of carbon nanotubes for NADH detection: an edge plane pyrolytic graphite electrode study. Analyst, 130(9), pp.1232-1239.

31. McCreery, R.L., (2008). Advanced carbon electrode materials for molecular electrochemistry. Chemical reviews, 108(7), pp.2646-2687.

32. Banerjee, S., Shim, J., Rivera, J., Jin, X., Estrada, D., Solovyeva, V., You, X., Pak, J., Pop, E., Aluru, N. and Bashir, R., (2012). Electrochemistry at the Edge of a Single Graphene Layer in a Nanopore. ACS nano, 7(1), pp.834-843.

33. Kamata, T., Kato, D., Hirono, S. and Niwa, O., (2013). Structure and electrochemical performance of nitrogen-doped carbon film formed by electron cyclotron resonance sputtering. Analytical chemistry, 85(20), pp.9845-9851.

34. Edwards, M.A., Bertoncello, P. and Unwin, P.R., (2009). Slow diffusion reveals the intrinsic electrochemical activity of basal plane highly oriented pyrolytic graphite electrodes. The Journal of Physical Chemistry C, 113(21), pp.9218-9223.

35. Unwin, P.R., (2014). Concluding remarks: there's nowt so queer as carbon electrodes. Faraday discussions, 172, pp.521-532.

36. Zhang, G., Kirkman, P.M., Patel, A.N., Cuharuc, A.S., McKelvey, K. and Unwin, P.R., (2014). Molecular functionalization of graphite surfaces: basal plane versus step edge electrochemical activity. Journal of the American Chemical Society, 136(32), pp.11444-11451.

37. Zhang, G., Cuharuc, A.S., Güell, A.G. and Unwin, P.R., (2015). Electrochemistry at highly oriented pyrolytic graphite (HOPG): lower limit for the kinetics of outer-sphere redox processes and general implications for electron transfer models. Physical Chemistry Chemical Physics, 17(17), pp.11827-11838.

38. Patel, A.N., Collignon, M.G., O'Connell, M.A., Hung, W.O., McKelvey, K., Macpherson, J.V. and Unwin, P.R., (2012). A new view of electrochemistry at highly oriented pyrolytic graphite. Journal of the American Chemical Society, 134(49), pp.20117-20130.

39. Lai, S.C., Patel, A.N., McKelvey, K. and Unwin, P.R., (2012). Definitive Evidence for Fast Electron Transfer at Pristine Basal Plane Graphite from High-Resolution Electrochemical Imaging. Angewandte Chemie International Edition, 51(22), pp.5405-5408.

40. Patel, A.N., Tan, S.Y. and Unwin, P.R., (2013). Epinephrine electro-oxidation highlights fast electrochemistry at the graphite basal surface. Chemical Communications, 49(78), pp.8776-8778.

41. Williams, C.G., Edwards, M.A., Colley, A.L., Macpherson, J.V. and Unwin, P.R., (2009). Scanning micropipet contact method for high-resolution imaging of electrode surface redox activity. Analytical chemistry, 81(7), pp.2486-2495.

42. Kirkman, P.M., Güell, A.G., Cuharuc, A.S. and Unwin, P.R., (2013). Spatial and temporal control of the diazonium modification of sp2 carbon surfaces. Journal of the American Chemical Society, 136(1), pp.36-39.

43. Anne, A., Cambril, E., Chovin, A., Demaille, C. and Goyer, C., (2009). Electrochemical atomic force microscopy using a tip-attached redox mediator for topographic and functional imaging of nanosystems. ACS nano, 3(10), pp.2927-2940.

44. Lhenry, S., Leroux, Y.R. and Hapiot, P., 2012. Use of catechol as selective redox mediator in scanning electrochemical microscopy investigations. Analytical chemistry, 84(17), pp.7518-7524.

45. Frederix, P.L., Bosshart, P.D., Akiyama, T., Chami, M., Gullo, M.R., Blackstock, J.J., Dooleweerdt, K., De Rooij, N.F., Staufer, U. and Engel, A., (2008). Conductive supports for combined AFM–SECM on biological membranes. Nanotechnology, 19(38), p.384004.

46. Randin, J. P., & Yeager, E. (1971). Differential capacitance study of stress-annealed pyrolytic graphite electrodes. Journal of the Electrochemical Society, 118(5), 711-714.

47. Wang, J., Yang, S., Guo, D., Yu, P., Li, D., Ye, J., & Mao, L. (2009). Comparative studies on electrochemical activity of graphene nanosheets and carbon nanotubes. Electrochemistry Communications, 11(10), 1892-1895.

48. Kaufmann, M., Zenkert, D., & Wennhage, P. (2010). Integrated cost/weight optimization of aircraft structures. Structural and Multidisciplinary Optimization, 41(2), 325-334.

49. Bråmå, T. (1987). Weight optimization of aircraft structures. In Computer Aided Optimal Design: Structural and Mechanical Systems (pp. 971-985). Springer Berlin Heidelberg.

50. Renton, W. J., Olcott, D., Roeseler, W., Batzer, R., Baron, W., & Velicki, A. (2004). Future of flight vehicle structures (2000 to 2023). Journal of Aircraft, 41(5), 986-998.

51. Alderliesten, R., & Benedictus, R. (2008). Fiber/metal composite technology for future primary aircraft structures. Journal of Aircraft, 45(4), 1182-1189.

52. Marsh, G. (2004). Composites lift off in primary aerostructures. Reinforced plastics, 48(4), 22-27.

53. Immarigeon, J. P., Holt, R. T., Koul, A. K., Zhao, L., Wallace, W., & Beddoes, J. C. (1995). Lightweight materials for aircraft applications. Materials Characterization, 35(1), 41-67.

54. Marsh, G. (2014). Composites and metals–a marriage of convenience?. Reinforced Plastics, 58(2), 38-42.

55. Soutis, C. (2005). Carbon fiber reinforced plastics in aircraft construction. Materials Science and Engineering: A, 412(1), 171-176.

56. Marsh, G. (2002). Composites strengthen aerospace hold. Reinforced Plastics, 46(7), 40-43.

57. Marsh, G. (2005). Airframers exploit composites in battle for supremacy. Reinforced Plastics, 49(3), 26-32.

58. Marsh, G. (2006). Duelling with composites. Reinforced Plastics, 50(6), 18-23.

59. Marsh, G. (2007). Airbus takes on Boeing with reinforced plastic A350 XWB. Reinforced plastics, 51(11), 26-29.

60. Marsh, G. (2010). Airbus A350 XWB update. Reinforced plastics, 54(6), 20-24.

61. Marsh, G. (2012). Aero engines lose weight thanks to composites. Reinforced Plastics, 56(6), 32-35.

62. Marsh, G. (2015). Composites in commercial jets. Reinforced Plastics, 59(4), 190-193.

63. Miller Jr, B. A. (1975). The galvanic corrosion of graphite epoxy composite materials coupled with alloys (No. GAE/MC/75D-8). AIR FORCE INST OF TECH WRIGHT-PATTERSON AFB OH SCHOOL OF ENGINEERING.

64. Miller, B. A., & Lee, S. G. (1976). The Effect of Graphite-Epoxy Composites on the Galvanic Corrosion of Aerospace Alloys (No. AFML-TR-76-121). AIR FORCE MATERIALS LAB WRIGHT-PATTERSON AFB OHIO.

65. Bellucci, F., Di Martino, A., & Liberti, C. (1986). Electrochemical behaviour of graphite-epoxy composite materials (GECM) in aqueous salt solutions. Journal of Applied Electrochemistry, 16(1), 15-22.

66. Bellucci, F. (1991). Galvanic corrosion between nonmetallic composites and metals: I effect of metal and of temperature. Corrosion, 47(10), 808-819.

67. Hihara, L. H., & Latanision, R. M. (1992). Galvanic corrosion of aluminum-matrix composites. Corrosion, 48(7), 546-552.

68. Mansfeld, F., & Parry, E. P. (1973). Galvanic corrosion of bare and coated Al alloys coupled to stainless steel 304 or Ti-6Al-4V. Corrosion Science, 13(8), 605-621.

69. Buarzaiga, M. M., & Thorpe, S. J. (1994). Corrosion Behavior of As-Cast, Silicon Carbide Particulate-Aluminum Alloy Metal-Matrix Composites. Corrosion, 50(3), 176-185.

70. Ireland, R., Arronche, L., & La Saponara, V. (2012). Electrochemical investigation of galvanic corrosion between aluminum 7075 and glass fiber/epoxy composites modified with carbon nanotubes. Composites Part B: Engineering, 43(2), 183-194.

71. Sloan, F. E., & Talbot, J. B. (1992). Corrosion of graphite-fiber-reinforced composites I-galvanic coupling damage. Corrosion, 48(10), 830-838.

72. Wielage, B., & Dorner, A. (1999). Corrosion studies on aluminium reinforced with uncoated and coated carbon fibres. Composites science and technology, 59(8), 1239-1245.

73. Fovet, Y., Pourreyron, L., & Gal, J. Y. (2000). Corrosion by galvanic coupling between carbon fiber posts and different alloys. Dental materials, 16(5), 364-373.

74. Brown, A. R. G., & Coomber, D. E. (1972). Behaviour of couples of aluminium and plastics reinforced with carbon fibre in aqueous salt solutions. British Corrosion Journal, 7(5), 232-235

75. Bozzini, B., & Fanigliulo, A. (2002). An electrochemical investigation into the galvanic corrosion of carbon steel coupled to carbon fibres. Materials and Corrosion, 53(12), 875-885.

76. Yuan, Y., Ahmed, J., & Kim, S. (2011). Polyaniline/carbon black composite-supported iron phthalocyanine as an oxygen reduction catalyst for microbial fuel cells. Journal of Power Sources, 196(3), 1103-1106.

77. Maldonado, S., & Stevenson, K. J. (2005). Influence of nitrogen doping on oxygen reduction electrocatalysis at carbon nanofiber electrodes. The Journal of Physical Chemistry B, 109(10), 4707-4716.

78. Ofoegbu, S.U. (2018). Corrosion and Corrosion Inhibition in Multi-material Combinations. (PhD. Thesis) University of Aveiro, Aveiro, Portugal.

79. Manne S. (1997) Visualizing self-assembly: Force microscopy of ionic surfactant aggregates at solid-liquid interfaces. In: Texter J. (eds) Amphiphiles at Interfaces. Progress in Colloid & Polymer Science, Vol. 103, 226-233.

80. Senden, T.J., Drummond, C.J. and Kekicheff, P., 1994. Atomic force microscopy: imaging with electrical double layer interactions. Langmuir, 10(2), pp.358-362.

81. Murray, R. W. (1992). Molecular design of electrode surfaces (Vol. 22). Wiley-Interscience.

82. Jaschke, M., Butt, H. J., Gaub, H. E., & Manne, S. (1997). Surfactant aggregates at a metal surface. Langmuir, 13(6), 1381-1384.

83. Wanless, E. J., & Ducker, W. A. (1997). Weak influence of divalent ions on anionic surfactant surface-aggregation. Langmuir, 13(6), 1463-1474.

84. Zhao, J., & Fung, B. M. (1993). NMR study of the transformation of sodium dodecyl sulfate micelles. Langmuir, 9(5), 1228-1231.

85. Reiss-Husson, F., & Luzzati, V. (1964). The structure of the micellar solutions of some amphiphilic compounds in pure water as determined by absolute small-angle X-ray

scattering techniques. The Journal of Physical Chemistry, 68(12), 3504-3511.

86. Király, Z., Findenegg, G. H., Klumpp, E., Schlimper, H., & Dékány, I. (2001). Adsorption calorimetric study of the organization of sodium n-decyl sulfate at the graphite/solution interface. Langmuir, 17(8), 2420-2425.

87. Manne, S., Cleveland, J. P., Gaub, H. E., Stucky, G. D., & Hansma, P. K. (1994). Direct visualization of surfactant hemimicelles by force microscopy of the electrical double layer. Langmuir, 10(12), 4409-4413.

88. Manne, S., & Gaub, H. E. (1995). Molecular organization of surfactants at solid-liquid interfaces. Science, 270(5241), 1480.

89. Wanless, E. J., & Ducker, W. A. (1996). Organization of sodium dodecyl sulfate at the graphite-solution interface. The Journal of Physical Chemistry, 100(8), 3207-3214.

90. Domínguez, H., (2009). Structure of the sodium dodecyl sulfate surfactant on a solid surface in different NaCl solutions. Langmuir, 25(16), pp.9006-9011.

91. Alias, M. N., & Brown, R. (1992). Damage to composites from electrochemical processes. Corrosion, 48(5), 373-378.

92. Taylor, S. R., Wall, F. D., & Cahen, G. L. (1996). The detection and analysis of electrochemical damage in bismaleimide/graphite fiber composites. Journal of The Electrochemical Society, 143(2), 449-458.

93. Alias, M. N., & Brown, R. (1993). Corrosion behavior of carbon fiber composites in the marine environment. Corrosion science, 35(1), 395-402.

94. Picquart, M. (1986). Vibrational model behavior of SDS aqueous solutions studied by Raman scattering. The Journal of Physical Chemistry, 90(2), 243-250.

95. Picquart, M., & Laborde, M. (1986). Raman Scattering in Aqueous Solutions of Sodium Dodecyl Sulfate. In Surfactants in Solution (pp. 189-201). Springer US.

96. Snyder, R. G., Hsu, S. L., & Krimm, S. (1978). Vibrational spectra in the C-H stretching region and the structure of the polymethylene chain. Spectrochimica Acta Part A: Molecular Spectroscopy, 34(4), 395-406.

97. Snyder, R. G., Strauss, H. L., & Elliger, C. A. (1982). Carbon-hydrogen stretching modes and the structure of n-alkyl chains. 1. Long, disordered chains. The Journal of Physical Chemistry, 86(26), 5145-5150.

98. Johnson, C. M., & Tyrode, E. (2005). Study of the adsorption of sodium dodecyl sulfate (SDS) at the air/water interface: targeting the sulfate headgroup using vibrational sum frequency spectroscopy. Physical Chemistry Chemical Physics, 7(13), 2635-2640.

99. Kalyanasundaram, K., & Thomas, J. K. (1976). The conformational state of surfactants in the

992 solid state and in micellar form. A laser-excited Raman scattering study. The Journal of
993 Physical Chemistry, 80(13), 1462-1473.
994
995 100. Siebert, H. (1957). Vibration of some sulfuric acid derivates. Z. anorg. allg. Chem, 289, 15-
996 28.
997
998 101. Okabayashi, H., Okuyama, M., Kitagawa, T., & Miyazawa, T. (1974). The Raman spectra
999 and molecular conformations of surfactants in aqueous solution and crystalline states.
1000 Bulletin of the Chemical Society of Japan, 47(5), 1075-1077.
1001
1002 102. Tiberg, F., Brinck, J., & Grant, L. (1999). Adsorption and surface-induced self-assembly of
1003 surfactants at the solid–aqueous interface. Current opinion in colloid & interface
1004 science, 4(6), 411-419.
1005
1006 103. Micklavzina, B.L., Zhang, S., He, H. and Longo, M.L., (2017). Nanomechanical
1007 Characterization of Micellar Surfactant Films via Atomic Force Microscopy at a Graphite
1008 Surface. Langmuir, 33(9), pp.2122-2132.
1009
1010 104. Chen, M., Burgess, I. and Lipkowski, J., (2009). Potential controlled surface aggregation
1011 of surfactants at electrode surfaces–A molecular view. Surface Science, 603(10-12),
1012 pp.1878-1891.
1013
1014 105. Randin, J.P. and Yeager, E., 1972. Differential capacitance study on the basal plane of
1015 stress-annealed pyrolytic graphite. Journal of Electroanalytical Chemistry and Interfacial
1016 Electrochemistry, 36(2), pp.257-276.
1017
1018 106. Morcos, I. and Yeager, E., 1970. Kinetic studies of the oxygen—peroxide couple on
1019 pyrolytic graphite. Electrochimica Acta, 15(6), pp.953-975.
1020
1021 107. Randin, J.P. and Yeager, E., 1975. Differential capacitance study on the edge orientation
1022 of pyrolytic graphite and glassy carbon electrodes. Journal of Electroanalytical Chemistry
1023 and Interfacial Electrochemistry, 58(2), pp.313-322.